One- and Two-Dimensional Nuclear Magnetic Resonance Spectroscopy with a Diamond Quantum Sensor

J. M. Boss,[1] K. Chang,[1] J. Armijo,[2] K. Cujia,[1] T. Rosskopf,[1] J. R. Maze,[2] and C. L. Degen[1,*]
[1]Department of Physics, ETH Zurich, Otto Stern Weg 1, 8093 Zurich, Switzerland
[2]Departmento de Física, Pontificia Universidad Católica de Chile, Santiago 7820436, Chile
(Received 10 December 2015; revised manuscript received 9 March 2016; published 9 May 2016)

We report on Fourier spectroscopy experiments performed with near-surface nitrogen-vacancy centers in a diamond chip. By detecting the free precession of nuclear spins rather than applying a multipulse quantum sensing protocol, we are able to unambiguously identify the NMR species devoid of harmonics. We further show that, by engineering different Hamiltonians during free precession, the hyperfine coupling parameters as well as the nuclear Larmor frequency can be selectively measured with up to five digits of precision. The protocols can be combined to demonstrate two-dimensional Fourier spectroscopy. Presented techniques will be useful for mapping nuclear coordinates in molecules deposited on diamond sensor chips, en route to imaging their atomic structure.

DOI: 10.1103/PhysRevLett.116.197601

Nitrogen-vacancy (NV) centers in diamond have opened exciting perspectives for the ultrasensitive detection of nuclear magnetic resonance (NMR), with possible applications to molecular structure imaging and chemical nanoanalytics [1–3]. NMR signals are detected by placing an analyte on a diamond chip engineered with a surface layer of NV centers and measuring the weak magnetic dipole fields of nuclei via optically detected magnetic resonance [4,5]. Examples of the rapid recent progress in NV NMR include the detection of small numbers of nuclei within voxels of a few $(\mathrm{nm})^3$ [6,7], the detection of multiple nuclear isotopes [8,9] and naturally occurring adsorption layers [6], the observation of surface diffusion and molecular motion [10,11], scanning imaging with <20 nm spatial resolution [9,12], and the spatial mapping of up to eight internal ^{13}C nuclei [13]. One of the far goals of NV NMR is the detection and three-dimensional mapping of individual nuclei in single molecules deterministically placed on the diamond chip [1,13,14].

Sensitive detection of nuclear magnetic signals is possible with multipulse sequences that consist of a series of π pulses [see Fig. 1(a)]. These sequences act like a narrowband lock-in amplifier [15] whose demodulation frequency $f = 1/(2\tau)$ is set by the delay time τ between the pulses [14,16,17]. By varying τ, a frequency spectrum of the magnetic field can be recorded. Multipulse spectroscopy of NMR signals has been reported for many nuclear isotopes, including ^{1}H, ^{13}C, ^{14}N, ^{15}N, ^{19}F, and possibly ^{29}Si and ^{31}P [3,6–9,12,18]. These experiments have, however, also revealed some important shortcomings of the method, including a modest spectral resolution [2,19] and ambiguities in peak assignments due to signal harmonics [18]. The fundamental reason for both effects is the indirect way nuclear spin signals are detected via their influence on the electronic spin.

A more natural way for measuring NMR signals is to observe the free nuclear precession reminiscent of the "free induction decay" in conventional NMR. The free nuclear precession can be detected via two consecutive nuclear spin measurements and incrementing the duration t_1 between the measurements. Mamin *et al.* [2] have demonstrated Fourier NMR by an electron-nuclear double resonance technique. Laraoui *et al.* [19] and others [10,11] have used two successive multipulse sequences to directly record the nuclear precession.

In the present work, we demonstrate two important applications of the free nuclear precession method: the unambiguous assignment of NMR peaks to nuclear isotopes and a set of measurements for determining nuclear hyperfine couplings with high precision. By combining two free-precession periods, we further demonstrate two-dimensional Fourier spectroscopy [21].

The basic sequence of a free nuclear precession experiment is shown in Fig. 1(b). The sequence consists of three propagators:

$$\hat{U}_{\mathrm{CP}}^{\dagger}\hat{U}_{\mathrm{free}}\hat{U}_{\mathrm{CP}}, \tag{1}$$

where $\hat{U}_{\mathrm{CP}}$ represents the traditional multipulse sequence [17] and $\hat{U}_{\mathrm{free}} = e^{-i\hat{H}_{\mathrm{free}}t_1}$ describes the period of free precession. $\hat{H}_{\mathrm{free}}$ is the free-precession Hamiltonian that is varied in our experiments. (Note that we use units of angular frequency). The measured "signal" is the probability p that the initial quantum state $|0\rangle$ of the electronic sensor spin is recovered after the three propagations:

$$p = |\langle 0|\hat{U}_{\mathrm{CP}}^{\dagger}\hat{U}_{\mathrm{free}}\hat{U}_{\mathrm{CP}}|0\rangle|^2 = |\langle a|\hat{U}_{\mathrm{free}}|a\rangle|^2, \tag{2}$$

where $|a\rangle = \hat{U}_{\mathrm{CP}}|0\rangle$ is the state after the $\hat{U}_{\mathrm{CP}}$ rotation.

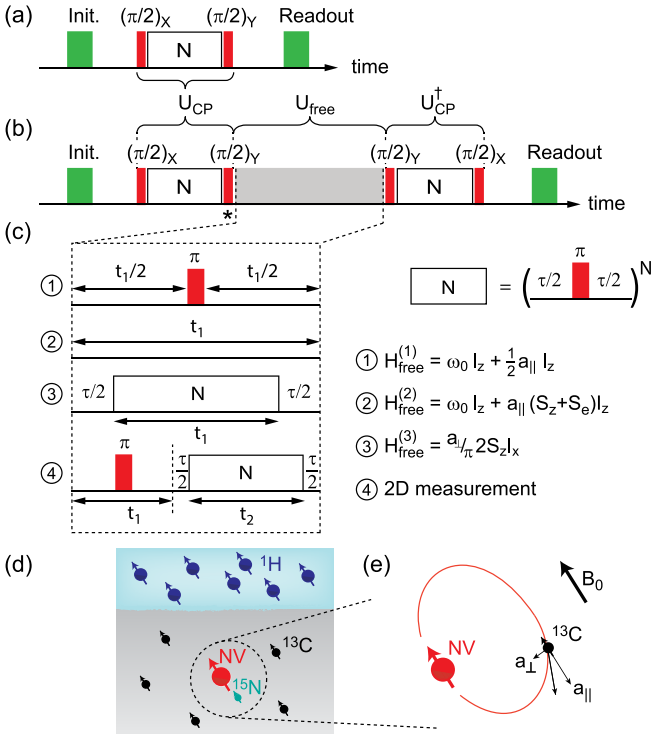

FIG. 1. (a) Pulse protocol for conventional multipulse spectroscopy. Laser pulses are colored green, and microwave pulses are colored red. The π pulse series used an $XY8$ phase pattern [20]. (b) Pulse protocol for a free nuclear precession measurement. The pulse marked by star was used for phase cycling (phases Y and $\bar{Y}$). (c) Free-precession sequences exploited in our experiments and corresponding Hamiltonians $\hat{H}_{\text{free}}^{(1\ldots3)}$. t_1 and t_2 are incremented evolution periods. The $\tau/2$ delays in ③ and ④ are used to adjust the axis of the nuclear Rabi rotation. (d) Sketch of the diamond chip with a near-surface NV center and ^{15}N, ^{13}C, and ^{1}H nuclei. (e) Vectorial picture of the parallel and transverse hyperfine parameters $a_{\parallel}$ and $a_{\perp}$. The contour represents a field line of the NV magnetic dipole.

Equation (2) contains the essence of the free-precession measurement. While conventional multipulse spectroscopy detects the electronic evolution $\hat{U}_{\text{CP}}$, with the signal given by $p = |\langle 0|\hat{U}_{\text{CP}}|0\rangle|^2$, the free-precession sequence measures the nuclear evolution $\hat{U}_{\text{free}}$ and simply applies $\hat{U}_{\text{CP}}$ and $\hat{U}_{\text{CP}}^{\dagger}$ to transform from and to the detectable electronic states $|0\rangle$ and $|1\rangle$.

We now explicitly calculate p for our experiment. For simplicity, we focus on the detection of a single nuclear spin. Moreover, we consider only the electronic subsystem $\{|0\rangle, |1\rangle\}$ that is resonant with the pulse sequence [22]. The basic Hamiltonian in the electron's rotating frame of reference is

$$\begin{aligned}\hat{H} &= \omega_0 \hat{I}_z + a_{\parallel}|1\rangle\langle 1|\hat{I}_z + a_{\perp}|1\rangle\langle 1|\hat{I}_x \\ &= \omega_0 \hat{I}_z + a_{\parallel}(\hat{S}_z + \hat{S}_e)\hat{I}_z + a_{\perp}(\hat{S}_z + \hat{S}_e)\hat{I}_x, \end{aligned} \quad (3)$$

where $\omega_0 = -\gamma_n B_0$ is the nuclear Zeeman frequency, γ_n is the nuclear gyromagnetic ratio, B_0 is the magnetic bias field, and $a_{\parallel}$ and $a_{\perp}$ are the parallel and transverse hyperfine coupling parameters, respectively [see Fig. 1(e)] [22,25]. $\hat{S}_z = \frac{1}{2}\{|1\rangle\langle 1| - |0\rangle\langle 0|\}$ and $\hat{S}_e = \frac{1}{2}\{|1\rangle\langle 1| + |0\rangle\langle 0|\}$ are spin operators on the electronic $\{|0\rangle, |1\rangle\}$ subsystem, and $\hat{I}_x$ and $\hat{I}_z$ are the nuclear spin operators. To include multiple nuclear spins, the Hamiltonian simply needs to be summed over the contributions of individual nuclei and possible internuclear interactions.

To analyze the effect of the three rotations $\hat{U}_{\text{CP}}^{\dagger}\hat{U}_{\text{free}}\hat{U}_{\text{CP}}$, it is convenient to represent the quantum state of the coupled spin system by its density operator. The density operator after initialization into $|0\rangle$ is $\hat{\sigma}_0 = |0\rangle\langle 0|\hat{I}_e = (\hat{S}_e - \hat{S}_z)\hat{I}_e$, where $\hat{I}_e$ is the identity. Omitting $\hat{S}_e$ and $\hat{I}_e$ for brevity, we have $\hat{\sigma}_0 = -\hat{S}_z$.

First, we apply the $\hat{U}_{\text{CP}}$ rotation. This rotation is implemented by a Carr-Purcell (CP) series of N equidistant π pulses that is sandwiched between two $\pi/2$ pulses, as shown in Fig. 1(c). If the delay time τ between π pulses is adjusted to one-half the nuclear Larmor period, $\tau = \pi/(\omega_0 + a_{\parallel}/2)$, the π pulses generate a nuclear Rabi rotation with an effective Hamiltonian $(a_{\perp}/\pi)2\hat{S}_z\hat{I}_x$ [22,26]. The overall effect of the $\hat{U}_{\text{CP}}$ sequence (including the $\pi/2$ pulses) is

$$\hat{\sigma}_a = |a\rangle\langle a| = \hat{U}_{\text{CP}}\hat{\sigma}_0\hat{U}_{\text{CP}}^{\dagger} = \cos(\omega_1 t)\hat{S}_x + \sin(\omega_1 t)2\hat{S}_z\hat{I}_x, \quad (4)$$

where $\omega_1 = a_{\perp}/\pi$ is the nuclear Rabi frequency and $t = N\tau$ the total duration of $\hat{U}_{\text{CP}}$. (Note that the expressions for τ and ω_1 are exact only in the limit of vanishing hyperfine coupling, $a_{\parallel}, a_{\perp} \ll \omega_0$. General expressions for arbitrary $a_{\parallel}$ and $a_{\perp}$ are provided in [22].)

The state $\hat{\sigma}_a$ is made up of two components: an electronic coherence $\hat{S}_x$ and a nuclear coherence $2\hat{S}_z\hat{I}_x$ that is conditional on the state of the electronic spin. We now look at the evolution of the two components under the Hamiltonian $\hat{H}_{\text{free}}$ [see Fig. 1(c) for examples]. If we restrict ourselves to Hamiltonians that commute with $\hat{S}_z$ (up to a sign change), the evolution is

$$\begin{aligned} p &= |\langle a|\hat{U}_{\text{free}}|a\rangle|^2 = \text{trace}(\hat{U}_{\text{free}}\sigma_a\hat{U}_{\text{free}}^{\dagger}\sigma_a) \\ &= \cos^2(\omega_1 t)\text{trace}(\hat{U}_{\text{free}}\hat{S}_x\hat{U}_{\text{free}}^{\dagger}\hat{S}_x) \\ &\quad + \sin^2(\omega_1 t)\text{trace}(\hat{U}_{\text{free}}\hat{I}_x\hat{U}_{\text{free}}^{\dagger}\hat{I}_x), \end{aligned} \quad (5)$$

where $\hat{U}_{\text{free}} = e^{-i\hat{H}_{\text{free}}t_1}$ and t_1 is the duration of free precession. To detect the desired nuclear evolution, we therefore simply need to record p as a function of time t_1 and pick out the $\hat{I}_x$ part of the signal. The latter can be achieved in several ways, for example, by phase cycling [see Fig. 1(b)] or by exploiting that the nuclear coherence is much longer lived than the electronic coherence [19].

Experiments were performed on an electronic-grade diamond chip with an ~5 nm deep layer of NV centers created by 2.5 keV $^{15}N^{+}$ ion implantation [see Fig. 1(d)]. The chip surface was patterned with an array of nanopillar waveguides [27]. The chip was integrated in a confocal

fluorescence microscope equipped with a 532 nm excitation laser and a photon-counting module. Laser pulses of 1.5 μs were used to initialize and read out the spin state of single NV centers, and microwave pulses passed through a nearby transmission line were used for spin manipulation. All measurements exploited the $m_S = 0 \leftrightarrow m_S = -1$ spin transition (corresponding to $|0\rangle$ and $|1\rangle$, respectively) and were carried out in a bias field of $\sim$0.18 T and at room temperature. The bias field was aligned with the NV symmetry axis to within a few degrees.

As a first application, we show that the $\hat{U}_{\mathrm{CP}}^{\dagger}\hat{U}_{\mathrm{free}}\hat{U}_{\mathrm{CP}}$ sequence can uniquely identify a NMR resonance and resolve ambiguities with harmonics affecting traditional multipulse spectroscopy [18]. To demonstrate this, we first record an extended multipulse spectrum using a simple $\hat{U}_{\mathrm{CP}}$ sequence [Fig. 2(a)]. The spectrum shows many peaks caused by the resonances of nuclear spins in the vicinity of the NV center. Some of the peaks [Figs. 2(c), 2(d), and 2(g)] can be tentatively assigned to ^{1}H, ^{13}C, and ^{15}N by consulting Table I. The other peaks [Figs. 2(b), 2(e), and 2(f)] have frequencies that are not found in the table, and it is not obvious which nuclear species they belong to.

Figures 2(b)–2(g) show spectra obtained with the $\hat{U}_{\mathrm{CP}}^{\dagger}\hat{U}_{\mathrm{free}}\hat{U}_{\mathrm{CP}}$ sequence. These spectra were recorded by tuning $\hat{U}_{\mathrm{CP}}$ (via adjusting τ) to one of the peaks labeled in Fig. 2(a), measuring the free precession for a series of t_1 values, and performing a Fourier transform with respect to t_1. We find that all Fourier spectra show peaks at expected NMR frequencies (Table I) and that we are now able to uniquely identify all nuclear species.

By comparing the frequencies between corresponding peaks in the multipulse and Fourier spectra, we can discriminate between different harmonics of the multipulse sequence. We find that both "ordinary" harmonics created at f/k and "spurious" harmonics appearing at $2f/k$ and $4f/k$ are present (where $k = 1, 3, 5, \ldots$). Ordinary harmonics are expected resonances of the multipulse filter function [14,16,17]. Spurious harmonics, by contrast, result from phase accumulation during π pulses and depend on many parameters, including π pulse duration, amplitude, and detuning [18].

Figure 3 shows another example of a multipulse spectrum alongside with two Fourier spectra. In the multipulse spectrum, three peaks are visible that partially overlap. The Fourier spectra reveal that the peaks are caused by the resonances of two nuclear species, including the second harmonic of a strongly coupled ^{13}C and the fundamental signal of a ^{1}H ensemble.

As a second application, we demonstrate that the $\hat{U}_{\mathrm{CP}}^{\dagger}\hat{U}_{\mathrm{free}}\hat{U}_{\mathrm{CP}}$ sequence allows for accurate measurements of the nuclear Zeeman frequency ω_0 as well as the two hyperfine parameters $a_{||}$ and $a_{\perp}$. A precise measurement of ω_0 is important to assign the nuclear species and to resolve weak additional effects, such as chemical shifts or nuclear dipole couplings. Accurate knowledge of $a_{||}$ and $a_{\perp}$ is critical for performing distance measurements on nuclei in a molecule.

To measure ω_0 and $a_{||}$, we perform a free-precession experiment without the central π pulse [Hamiltonian $\hat{H}_{\mathrm{free}}^{(2)}$ in Fig. 1(c)]. The nuclear evolution now becomes conditional on the state of the electronic spin: If the electron is in state $|0\rangle$, the hyperfine interaction is absent and the nucleus precesses with frequency ω_0. By contrast, if the electron is in state $|1\rangle$, the hyperfine interaction is present and the nuclear precession frequency is $\omega_0 + a'_{||}$ [22]. A beating pattern is seen in the time evolution [Fig. 4(a)], and two peaks appear after Fourier transformation [Fig. 4(b)], reflecting the two frequencies. By comparison, the conventional multipulse spectrum shows only a single broad peak at $\omega_0 + a'_{||}/2$ [Fig. 4(b)]. We have written $a'_{||}$ to emphasize

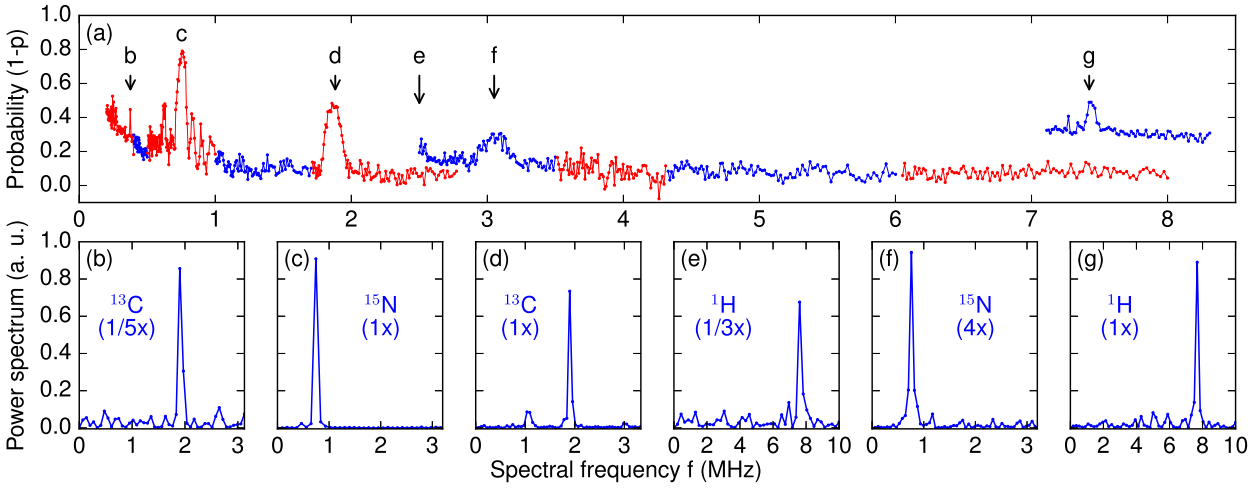

FIG. 2. Unambiguous identification of NMR signals: (a) Multipulse spectrum in a field of $B_0 = 174$ mT. Colors identify different data sets. (b)–(g) Fourier spectra for the six peaks labeled in (a). All spectra used Hamiltonian $\hat{H}_{\mathrm{free}}^{(1)}$, except for (d) and (e) that used $\hat{H}_{\mathrm{free}}^{(2)}$ [see Fig. 1(c)]. The nuclear species and multipulse harmonic are indicated for each spectrum. The ^{15}N peak is present due to a small misalignment of the external bias field.

TABLE I. NMR frequencies for the nuclear spin species detected in the experiment. For ^{15}N, two resonances are possible that are split by a hyperfine coupling of 3.05 MHz.

Isotope	NMR frequency (at 174 mT)
^{1}H	7.40 MHz
^{13}C	1.86 MHz
^{15}N	0.75 MHz, 2.30 MHz

that the measured frequencies are slightly different from the exact $a_{||}$ [Eq. (3)] because of our approximation that $a_{||}$, $a_{\perp} \ll \omega_0$ [22].

By applying a train of π pulses (Hamiltonian $\hat{H}^{(3)}_{\text{free}}$) [28], we can also measure the transverse coupling parameter $a_{\perp}$ [see Figs. 4(c) and 4(d)]. As with the CP sequence, the π pulses induce a nuclear Rabi rotation with frequency $\omega_1 = a'_{\perp}/\pi$ from which $a'_{\perp}$ can be extracted. Again, because of our approximation that $a_{||}$, $a_{\perp} \ll \omega_0$, the measured $a'_{\perp}$ will deviate from the exact $a_{\perp}$ [22].

In both of the above measurements, the nuclear coherence is maintained for much longer than the electronic T_2 time (here $T_2 \sim 10$ μs). This is because the $2\hat{S}_z\hat{I}_x$ state in (4) and (5) is insensitive to electronic decoherence and affected only by electronic spin flips or nuclear decoherence. In our experiments, the state lifetime was limited by electronic spin flips with $T_1 \sim 0.2$ ms. This constitutes an $\sim$20$\times$ improvement compared to the lifetime of the electronic coherence. The lifetime could be extended further by storing the state $\hat{S}_z$ in an auxiliary nuclear spin during free precession [19,29].

The long free-precession times allow for a high measurement accuracy of the hyperfine parameters. As shown in Fig. 4 and Ref. [22], frequencies can be measured with up to five digits of precision. We have calculated the exact $a_{||}$ and $a_{\perp}$ for the ^{13}C of Fig. 4, taking into account that $a_{||}$, $a_{\perp} \ll \omega_0$ is not fulfilled [22]. The resulting values are $a_{||}/2\pi = 4.001\,95(30)$ MHz and $a_{\perp}/2\pi = 0.5132(17)$ MHz [22]. Tentatively, this ^{13}C can be assigned to lattice site E, F in Ref. [30]. The radial distance of these sites is about $r \sim 3$ Å. Although one could, in principle, use $a_{||}$ and $a_{\perp}$ to calculate a precise distance and internuclear angle based on the dipolar interaction [22], this calculation is inaccurate for the present ^{13}C due to a significant Fermi contact contribution.

Finally, we demonstrate that two hyperfine measurements can be combined to record two-dimensional (2D) Fourier spectra [21,31,32]. Two-dimensional spectroscopy is an important technique in magnetic resonance for determining the connectivity in a spectrum [33,34]. As a proof of principle, we demonstrate that $a_{||}$ and $a_{\perp}$ spectra can be correlated. During a first period t_1 we apply Hamiltonian $\hat{H}^{(1)}_{\text{free}}$ followed by a period t_2 of with Hamiltonian $\hat{H}^{(3)}_{\text{free}}$ [see Fig. 1(c)]. We then increment the evolution times t_1 and t_2 to produce a two-dimensional

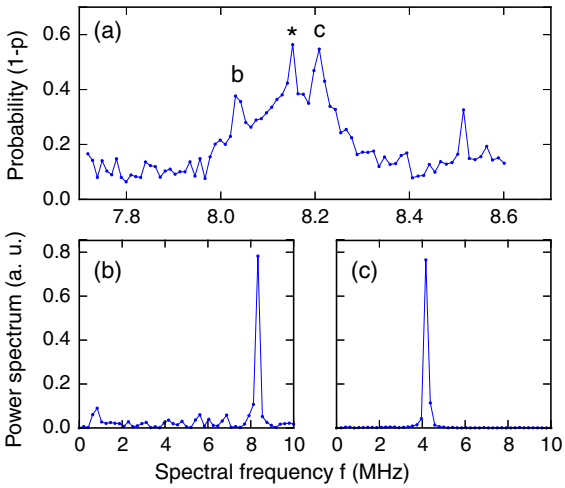

FIG. 3. (a) Multipulse spectrum and (b),(c) Fourier spectra at $\sim$8 MHz. Two signals are present: one produced by the fundamental resonance of a ^{1}H ensemble (b) and one produced by the second harmonic of a strongly coupled ^{13}C nucleus (c). The third peak (star) in (a) is caused by the same ^{13}C (data not shown). The number of pulses applied during $\hat{U}_{\text{CP}}$ was $N = 1200$ in (a), 720 in (b), and 1000 in (c).

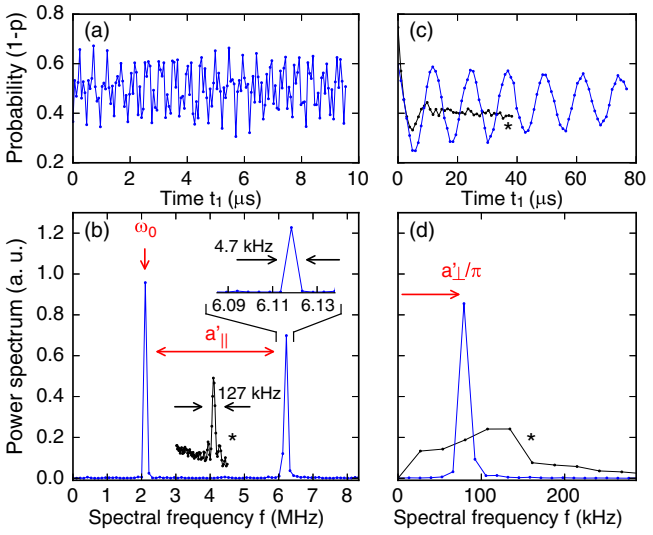

FIG. 4. Precision measurement of ω_0, $a_{||}$, and $a_{\perp}$ obtained by observing the nuclear, rather than the electronic, evolution. The same ^{13}C as in Fig. 3 is being studied. (a) Free-precession signal under Hamiltonian $\hat{H}^{(2)}_{\text{free}}$. (b) Fourier spectrum of (a) showing two peaks at ω_0 and $\omega_0 + a'_{||}$. The enlargement on the upper peak shows a high-resolution spectrum obtained from an undersampled data set (see [22]), with t_1 up to 200 μs. (Star) shows a traditional multipulse spectrum for comparison. Deduced parameters are $\omega_0/2\pi = 2.093\,20(11)$ MHz and $a'_{||}/2\pi = 4.023\,50(16)$ MHz [22]. (c) Free-precession signal under Hamiltonian $\hat{H}^{(3)}_{\text{free}}$. (Star) shows the corresponding multipulse signal obtained by incrementing the number of π pulses $N = t_1/\tau$. (d) Fourier spectra of the two curves from (c). The deduced parameter is $a'_{\perp}/2\pi = 0.250\,70(41)$ MHz. Measurement uncertainties are fit errors [22].

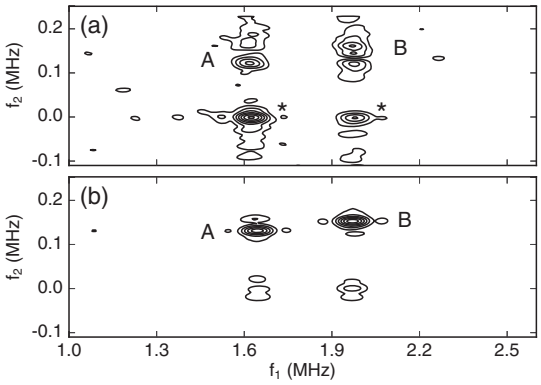

FIG. 5. Two-dimensional Fourier NMR spectrum (absolute value) of two ^{13}C nuclei labeled by "A" and "B." (a) is the measurement, and (b) is a simulation. The f_1 dimension plots $\omega_0 + a'_{||}/2$ and the f_2 dimension plots $a'_{\perp}/\pi$. Dwell time was 120 ns (120 increments) for f_1 and 2168 ns (40 increments) for f_2. The peaks marked by star are present because the phase of the nuclear Rabi rotation was not perfectly adjusted. The total measurement time was 16 h.

data set that results, after a two-dimensional Fourier transform, in the spectrum shown in Fig. 5.

In summary, the concept of "free nuclear precession" has been implemented to demonstrate several important new capabilities in diamond-based NMR spectroscopy. Spectral peaks could be uniquely assigned to nuclear isotopes, thereby resolving critical ambiguities with multipulse quantum sensing sequences. Selective and highly precise measurements of Zeeman and hyperfine frequencies were introduced, and 2D Fourier spectroscopy was demonstrated to add further spectral resolution. Together, the two methods will allow assigning many more nuclei in outside molecules than is possible with conventional detection schemes.

The authors thank Matthew Markham and Andy Edmonds for the custom diamond chip and Tim Taminiau for helpful discussions. This work was supported by Swiss NSF Project Grant No. 200021_137520, the NCCR QSIT, and the DIADEMS program 611143 of the European Commission.

*degenc@ethz.ch

[1] C. L. Degen, Appl. Phys. Lett. **92**, 243111 (2008).
[2] H. J. Mamin, M. Kim, M. H. Sherwood, C. T. Rettner, K. Ohno, D. D. Awschalom, and D. Rugar, Science **339**, 557 (2013).
[3] T. Staudacher, F. Shi, S. Pezzagna, J. Meijer, J. Du, C. A. Meriles, F. Reinhard, and J. Wrachtrup, Science **339**, 561 (2013).
[4] G. Davies and M. F. Hamer, Proc. R. Soc. A **348**, 285 (1976).
[5] A. Gruber, A. Drabenstedt, C. Tietz, L. Fleury, J. Wrachtrup, and C. von Borczyskowski, Science **276**, 2012 (1997).
[6] M. Loretz, S. Pezzagna, J. Meijer, and C. L. Degen, Appl. Phys. Lett. **104**, 033102 (2014).
[7] C. Muller, X. Kong, J. M. Cai, K. Melentijevic, A. Stacey, M. Markham, D. Twitchen, J. Isoya, S. Pezzagna, J. Meijer, J. F. Du, M. B. Plenio, B. Naydenov, L. P. McGuinness, and F. Jelezko, Nat. Commun. **5**, 4703 (2014).
[8] S. J. Devience, L. M. Pham, I. Lovchinsky, A. O. Sushkov, N. Bar-gill, C. Belthangady, F. Casola, M. Corbett, H. Zhang, M. Lukin, H. Park, A. Yacoby, and R. L. Walsworth, Nat. Nanotechnol. **10**, 129 (2015).
[9] T. Haberle, D. Schmid-Lorch, F. Reinhard, and J. Wrachtrup, Nat. Nanotechnol. **10**, 125 (2015).
[10] X. Kong, A. Stark, J. Du, L. P. McGuinness, and F. Jelezko, Phys. Rev. Applied **4**, 024004 (2015).
[11] T. Staudacher, N. Raatz, S. Pezzagna, J. Meijer, F. Reinhard, C. A. Meriles, and J. Wrachtrup, Nat. Commun. **6**, 8527 (2015).
[12] D. Rugar, H. J. Mamin, M. H. Sherwood, M. Kim, C. T. Rettner, K. Ohno, and D. D. Awschalom, Nat. Nanotechnol. **10**, 120 (2015).
[13] R. Schirhagl, K. Chang, M. Loretz, and C. L. Degen, Annu. Rev. Phys. Chem. **65**, 83 (2014).
[14] N. Zhao, J. L. Hu, S. W. Ho, J. T. K. Wan, and R. B. Liu, Nat. Nanotechnol. **6**, 242 (2011).
[15] S. Kotler, N. Akerman, Y. Glickman, A. Keselman, and R. Ozeri, Nature (London) **473**, 61 (2011).
[16] L. Cywinski, R. M. Lutchyn, C. P. Nave, and S. D. Sarma, Phys. Rev. B **77**, 174509 (2008).
[17] G. D. Lange, D. Riste, V. V. Dobrovitski, and R. Hanson, Phys. Rev. Lett. **106**, 080802 (2011).
[18] M. Loretz, J. M. Boss, T. Rosskopf, H. J. Mamin, D. Rugar, and C. L. Degen, Phys. Rev. X **5**, 021009 (2015).
[19] A. Laraoui, F. Dolde, C. Burk, F. Reinhard, J. Wrachtrup, and C. A. Meriles, Nat. Commun. **4**, 1651 (2013).
[20] T. Gullion, D. B. Baker, and M. S. Conradi, J. Magn. Reson. **89**, 479 (1990).
[21] W. P. Aue, E. Bartholdi, and R. R. Ernst, J. Chem. Phys. **64**, 2229 (1976).
[22] See Supplemental Material at http://link.aps.org/supplemental/10.1103/PhysRevLett.116.197601 for a definition of hyperfine parameters and the fitting procedure, which includes Refs. [23,24].
[23] G. A. F. Seber and C. J. Wild, *Statistical Inference* (Wiley, New York, 2005), pp. 191–269, ISBN .
[24] A. Gali, M. Fyta, and E. Kaxiras, Phys. Rev. B **77**, 155206 (2008).
[25] T. H. Taminiau, J. J. T. Wagenaar, T. V. der Sar, F. Jelezko, V. V. Dobrovitski, and R. Hanson, Phys. Rev. Lett. **109**, 137602 (2012).
[26] T. H. Taminiau, J. Cramer, T. van der Sar, V. V. Dobrovitski, and R. Hanson, Nat. Nanotechnol. **9**, 171 (2014).
[27] T. M. Babinec, B. J. M. Hausmann, M. Khan, Y. Zhang, J. R. Maze, P. R. Hemmer, and M. Loncar, Nat. Nanotechnol. **5**, 195 (2010).
[28] M. S. Blok, N. Kalb, A. Reiserer, T. H. Taminiau, and R. Hanson, Faraday Discuss. **184**, 173 (2015).
[29] T. Rosskopf (unpublished).
[30] B. Smeltzer, L. Childress, and A. Gali, New J. Phys. **13**, 025021 (2011).
[31] M. Kost, J. Cai, and M. B. Plenio, Sci. Rep. **5**, 11007 (2015).
[32] W. L. Ma and R. B. Liu, arXiv:1512.03548.
[33] R. R. Ernst, G. Bodenhausen, and A. Wokaun, *Principles of Nuclear Magnetic Resonance in One and Two Dimensions*, International Series of Monographs on Chemistry (Clarendon, Oxford, 1990).
[34] K. Wuthrich, J. Biomol. NMR **27**, 13 (2003).